JOURNAL OF Applied Polymer SCIENCE

Mechanical properties and *in vitro* degradation behavior of additively manufactured phosphate glass particles/fibers reinforced polylactide

Lizhe He, Jiahui Zhong, Chenkai Zhu, Xiaoling Liu
University of Nottingham Ningbo China, Ningbo 315100, China
Correspondence to: X. Liu (E-mail: xiaoling.liu@nottingham.edu.cn)

ABSTRACT: Phosphate glass/polylactide (PG/PLA) composites were additively manufactured via fused deposition modeling. The incorporation of 10 wt % PG particles improved the flexural modulus of composites by ~14% (3.53 GPa) but led to 5% reduction in flexural strength (92.4 MPa). The trend was more pronounced as the particle loading doubled. Comparing to a particulate composite of the same weight fraction, milled PG fibers (PGFs) reinforcement led to more effectively improved flexural modulus (~30%, 4.10 GPa). After 28 days of *in vitro* degradation in phosphate buffered saline, the particulate composites lost more than 30% of their initial mechanical properties, in contrast to less than 10% reduction of strength/modulus reported from fiber reinforced composites. The additively manufactured PG/PLA matrix composites have potential for application as customized bone fixation plates to repair the fractures under modest load-bearing applications. © 2019 The Authors. *Journal of Applied Polymer Science* published by Wiley Periodicals, Inc. J. Appl. Polym. Sci. **2019**, *136*, 48171.

KEYWORDS: additive manufacturing; biodegradable composites; mechanical properties; phosphate-based glass; polylactide

Received 15 February 2019; accepted 2 June 2019
DOI: 10.1002/app.48171

INTRODUCTION

Internal fixation is one of the most common practices in the healing of bone fractures. With the implantation of devices such as bone fixation plates, screws, pins, and intramedullary rods, the fractured pieces of bones are held together, stabilized for a several weeks so the regeneration of bones take place that eventually leads to union of the fracture.[1,2]

In order to repair the fracture with high stability and safety without medical complications (e.g., irritating the biological system,[3] secondary bone fractures due to "stress shielding,"[4] and failed restoration of bone function[5]), both the material properties and design fixation device are critical. Clearly, materials must be biocompatible but biofidelic stiffness is also desirable and, ideally, biodegradability that would eliminate the need for surgery to remove the implant after healing is accomplished.[6] As for the design and fabrication, an internal fixation implant with shape and size that specifically fit the anatomy of the patient is desirable for the safe and effective restoration of bone functions, without leading to complications such as malreduction and tissue irritation.[7]

One potential approach to fabricate fixation implant with the desired form and function is to fabricate the biomaterials via additive manufacturing. Here, a "sliced" digital model is fabricated into solid product via the layer-by-layer addition of materials. The process is automated, offers high precision and the ability to fabricate complex geometries. As such, the physiochemical and biological properties of biomaterials can be exploited along with customized geometries/structures attributed which add functionality in clinical applications. For example, the pore size and porosity can be finely controlled to produce tissue engineering scaffolds which optimize bone ingrowth while maintaining acceptable mechanical strength and degradation rate[8]; the geometries of additively manufactured (e.g.,) tricalcium phosphate/polycaprolactone bone graft can be contoured to suit the defect site thus facilitating the implantation process and improving bone stability, while the material composition contributes to efficient bone-bonding bioactivity and complete biodegradability.[9,10]

Inspired by the success in additive manufacturing of biodegradable polymer [e.g., polylactide (PLA)[11,12] and polycaprolactone[10,13]] reinforced with bioactive particulate reinforcements (e.g., hydroxyapatite,[11] tricalcium phosphate,[14] and bioactive glass[12,15]), this work aims to investigate the additive manufacturing of phosphate glass (PG) reinforced PLA composites for their potential as bone fixation plates. It is previously reported that compression molded PG/PLA composites exhibit bone-mimetic mechanical properties and complete biodegradability, making them potential materials for resorbable fracture

fixation plates.[16,17] However, the PG/PLA composites are conventionally fabricated by die forming (i.e., compression molding) and as such are constrained by the mold geometry, which is unlikely to be patient-specific. Meanwhile, the PLA matrix is brittle and has poor tolerance for mechanical deformation[18]; otherwise, machining of fiber composites leads to direct exposure of fibers to the biological system, resulting in rapid loss of mechanical properties due to interface degradation.[17,19] These factors mitigate against geometric modification of composite fracture plates in clinical applications. However, additive manufacturing introduces a relatively straightforward for customized composite implants with potential advantages including improved implant fit and simplified clinical procedures.[20]

In this study, the PG/PLA composites were fabricated via fused deposition modeling (FDM), and the flexural mechanical properties as well as the *in vitro* degradation behavior characterized. Comparisons were made with PLA, and PLA reinforced with different loadings of PG particles (PGPs) as well as composites with reinforcements of different geometries [PGPs or milled phosphate glass fibers (PGFs)]. The ultimate aim is to evaluate the prospect of additively manufactured composites as fracture fixation plates.

EXPERIMENTAL

Materials

Glass precursors, including phosphorous pentoxide, boron oxide, calcium hydrogen phosphate dihydrate ($2H_2O$), magnesium hydrogen phosphate trihydrate, sodium dihydrogen phosphate dehydrate ($2H_2O$), potassium dihydrogen phosphate, and iron (III)-phosphate tetrahydrate sourced from Sigma-Aldrich (St. Louis, MO, United States). PGF yarns with the chemical composition of P48-B12-Ca14-Mg17-Na1-Fe8 (the numbers indicate the molar percentage of each oxide of elements in the phosphate glass network) was supplied by Sinoma Co., Ltd. (Nanjing, China).[21] The PLA used in this study was the Ingeo 4043D (NatureWorks, Minnetonka, MN, United States) in the form of granules. Phosphate buffered saline (PBS) was prepared from tablets (P4417-100TAB; Sigma-Aldrich, St. Louis, MO, United States) in the ratio of one tablet: 200 mL deionized water.

Preparation of PGPs and Milled Fibers

Phosphate glass and glass fibers with identical chemical composition as P48-B12-Ca14-Mg17-Na1-Fe8 were used. Phosphate glass was prepared following the protocol described elsewhere.[22] Briefly, the glass precursors were weighed, blended in the platinum crucible and isothermally heated at 300 °C for 30 min to remove moisture. The mixture was then transferred into a muffle furnace (1400X; Kejing, Hefei, China) where it was heated to 1200 °C for 90 min. The resulting glass melt was cast into a stainless-steel mold and cooled to room temperature. The glass casting was crushed using a high-speed blade mill (DY1000; Xinyuan, Hebi, China) into powders, and further milled with an ultracentrifugal mill (ZM-200; Retsch, Haan, Germany) equipped with a 150 μm sieve. The continuous PGF yarns were trimmed manually into ~10 mm short fiber bundles, then milled with the same ultracentrifugal mill.

Table I. Key Parameters of the FDM Process

Parameters	Value/setting
Nozzle diameter	0.4 mm
Extrusion ratio	120%
Layer height	0.2 mm
Build plate temperature	60 °C
Nozzle temperature	235 °C (PLA)/255 °C (other composites)
Infill pattern	0° rectilinear (test specimens)
Infill ratio	100% (test specimens)
Default printing speed	3000 mm min^{-1}

Preparation of Composite Masterbatch

A masterbatch—dilution process was applied to obtain FDM feedstock with the desired ratio of fillers. The masterbatch was prepared by melt-blending PLA and with either milled fibers or particulate filler in a twin-screw extruder (TSH-25; Chuangbo, Nanjing, China) and chopped into pellets. Before use, the PLA granules and milled fibers/particulate filler were dried at 50 °C for 48 h. PLA granules were then fed into the twin-screw extruder via the main hopper, while the fillers were introduced via the side hopper. The six heating chambers of the extruder were set from 175 to 205 °C, and the screw rotation rate was 20 rpm. The extrudates were then water cooled and chopped into pellets. Loss on ignition confirmed the weight fractions for the masterbatches at 28 wt % (particulate) and 17 wt % (milled fiber), respectively. Unreinforced PLA pellets were produced following the same protocol.

Preparation of Three-Dimensional Printing Filaments

The unreinforced PLA pellets and the masterbatches were weight and dry mixed to obtain four different blends: pure PLA, composites with 10 wt % PGP 10, 20 wt % PGP 20, and 10 wt % PGF 10. These blends were then processed using a filament extruder (Model C-2; Wellzoom, Shenzhen, China) equipped with a 2.0 mm extrusion die. The preheating zone and extrusion die temperatures were set at 193 and 187 °C, respectively. The extruded filaments with a diameter of 1.75 ± 0.15 mm were water cooled prior to winding.

Three-Dimensional Printing via FDM

Three-dimensional models, including three-point bending test specimens based on ISO 14125:1998 standard ($L \times D \times H = 80 \times 10 \times 4\ mm^3$) and dynamic mechanical test specimens ($L \times D \times H = 25 \times 8 \times 2\ mm^3$) were designed using PTC Creo Parametric (Version 4.0; PTC Software, Boston, MA, United States) and saved as stereolithography (STL) files. The STL files were then imported into Simplify3D (Version 4.0.3; Simplify3D, Blue Ash, OH, United States) to configure the FDM process, with the key parameters listed in Table I. The configured FDM programs were then transferred to the FDM device (Ultimaker 2+; Ultimaker, Geldermalsen, Netherlands) to be fabricated. The FDM extrusions were mainly in the 0° direction (along the 80 mm edges), which was vertical to the crosshead movement in the three-point bending test.

Three-Point Bending Test

The three-point bending test specimens were tested according to the ISO 14125:1998 test standard, using a universal testing machine (E45.105; MTS, Eden Prairie, MO, United States) equipped with a 50 kN load cell. The span of the fixture was 64 mm, and the crosshead speed was set at 2 mm min^{-1}. The tests

were carried out with five replicates using virgin test specimens, and three replicates for degraded specimens over a 56-day period (see In Vitro Degradation section).

In Vitro Degradation

In vitro degradation was carried out to evaluate the mechanical properties and hydroscopy of the composites after hydrolytic degradation. Three-point bending test specimens were placed into glass vials filled with 20 mL of PBS with initial pH value of 7.4 ± 0.1. The specimens were then maintained at 37 °C, and every 7 days, the PBS was refreshed.

Test specimens were removed from the media at predetermined intervals, surface dried, and weighed to establish moisture retention prior to flexural testing. After three-point bending test, the specimens were dried at 40 °C for 1 week to determine the dry mass and the consequent water uptake.

pH Value

The pH values of immersion media were monitored in order to gauge the degradation the specimens. After calibration using three types of standard calibration solutions (pH = 4.01, 7.00, and 9.21 at 25 °C), pH values were measured using a pH meter (FE28-Meter; Mettler Toledo, Columbus, OH, United States).

Dynamic Mechanical Analysis

Dynamic mechanical analysis (DMA) was carried out in the dynamic mechanical analyzer (DMA8000; Perkin-Elmer, Waltham, MA, United States) using single cantilever bending specimens with a temperature scanning process applied. During the tests, the specimens were cycled with constant strain of 0.05% at a frequency of 1 Hz, while being ramped from 30 to 80 °C at 2 °C min^{-1}. The storage modulus (E) and loss factors (tan δ) were recorded, and the temperature where loss factor peaked was determined as glass-transition temperature (T_g). Each material variant was tested with three replicates before and after 3 days of *in vitro* degradation.

Scanning Electron Microscopy and Energy-Dispersive Spectroscopy

The fracture surfaces and polished cross section of specimens were imaged via scanning electron microscopy (SEM). For the polished cross sections, a cross-sectional surface vertical to the long edge was made with a diamond saw before polishing with 1000-mesh sanding disks first, then with 5000-mesh sanding disks using the an orbital polisher (YMP-1; Yuzhou, Shanghai, China). The pristine fracture surfaces and polished cross sections were then sputter coated with 10 nm gold layer using the vacuum coating system (SCD-500; Leica Microsystems, Wetzlar, Germany), and imaged using the SEM (Sigma VP; Zeiss, Oberkochen, Germany) in secondary electron mode. Energy-dispersive spectroscopy (EDS) spectra based on SEM images were acquired under the accelerating voltage of 20 kV using the X-act silicon drift detector (Oxford Instruments, Oxford, UK).

Fiber Length Analysis

Milled PGF extracted from PGF 10 composites were imaged via an electronic optical microscope (NE930; Nexcope, Ningbo, China) with their images captured using the ScopeImage software (Version 9.0, Shareware). For the measurements of fiber length, the images were processed with Fiji distribution of ImageJ (ImageJ 1.52e, developed by Wayne Rasband from US National Institutes of Health) using the plugin "ridge detection" (developed by Thorsten Wagner and Mark Hiner).

Laser Particle Size Analysis

The size distribution of PGPs was characterized using a laser particle size analyzer (Bettersize 2000; Bettersize, Dandong, China). Around 0.5 g PGPs (conditioned at 100 °C for 24 h) were added to the dispersion media reservoir which was prefilled with deionized water. The slurry was then mechanically stirred and sonicated, until no agglomerates of PGPs were seen and the obscuration value fluctuated around 15%. The particle size measurement was then carried out, and the volume-based particle size distribution was thus obtained.

Statistical Analysis

Statistical analysis was performed using the GraphPad Prism (Version 7.00; GraphPad Software, San Diego, CA, United States). Unpaired, two-tailed t tests were carried out using the data acquired, with a confidence level of 95% ($p < 0.05$ defined as statistical significance).

RESULTS

Characterization of PGPs and Milled PGFs

The milled glass particles are shown in Figure 1(a) with the particle size distribution shown in Figure 1(b). The D50 value (indicating the median particle sizes) was 31 μm and 90% of the particles were below 68 μm (D90).

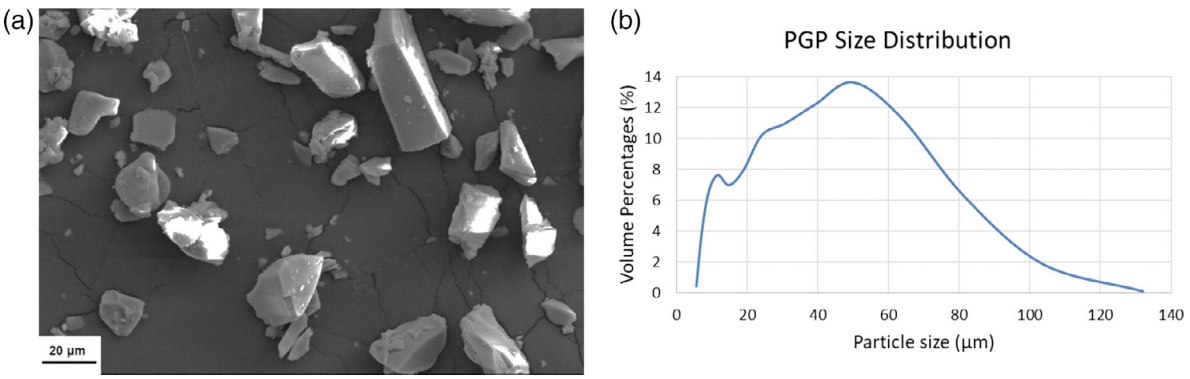

Figure 1. SEM image (a) and particle size distribution (b) of PGPs. [Color figure can be viewed at wileyonlinelibrary.com]

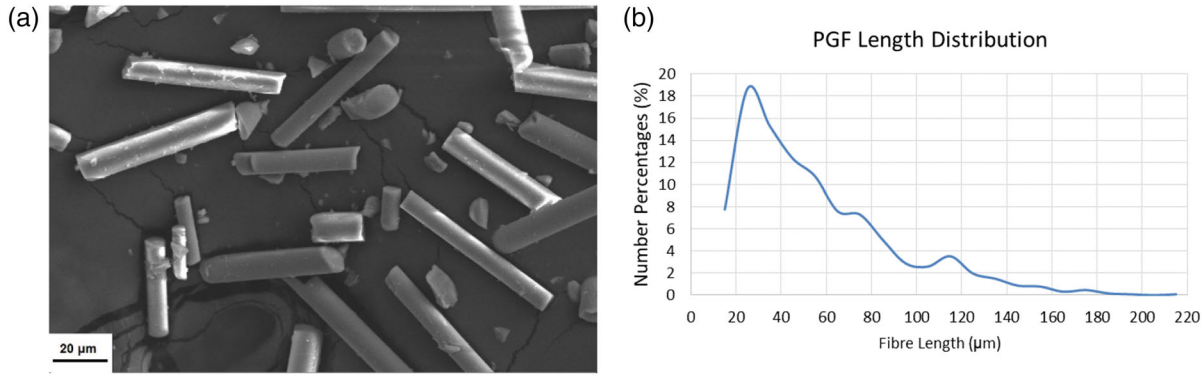

Figure 2. SEM image (a) and fiber length distribution (b) of milled PGPs. [Color figure can be viewed at wileyonlinelibrary.com]

The SEM image and length distribution of the milled fibers are shown in Figure 2. The average fiber length (±standard deviation) was 54.69 ± 34.32 μm. The median fiber length was 44.92 μm, and the mode was 27 μm. More than 50% of the fibers were less than 50 μm, and 90% of the fibers less than 110 μm.

Initial Flexural Properties

The initial flexural properties of FDM fabricated composites are shown in Figure 3. The flexural strength and modulus of pure PLA specimens were 97.20 ± 3.27 MPa and 3.13 ± 0.20 GPa, respectively. With the addition of 10 wt % PGPs, the flexural strength decreased by 5.0% (92.38 ± 3.04 MPa), whereas the flexural modulus was enhanced by 12.8% (3.53 ± 0.23 GPa). The trend was more pronounced with 12.5% strength reduction (85.98 ± 2.91 MPa) and 31.9% modulus increment (4.13 ± 0.16 GPa) as the PGP loading doubled, and both the strength reduction and the modulus increment were found with statistical significance ($p < 0.05$, $n = 5$).

Similar to the PG particles, the incorporation of 10 wt % milled fibers led to a strength reduction of 5.1% (92.28 ± 4.07 MPa). However, the flexural modulus was significantly improved by 31.0% (4.10 ± 0.57 GPa) compared to unreinforced PLA. Strong statistical significance ($p < 0.01$) was confirmed comparing the flexural modulus of PGF 10 composites with either PLA or PGP 10 composites, suggesting a more pronounced stiffening effect from the addition of fibers.

Typical stress–strain curves for all specimens are given in Figure 4. Typically, an initial linear portion indicating elastic deformation preceded the onset of yielding at around 2% strain. Finally, the stress dropped abruptly, marking the fractures of specimens. The PLA

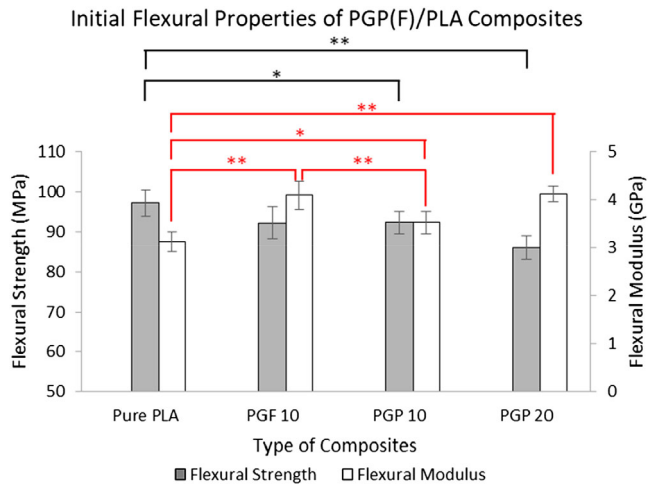

Figure 3. Initial flexural properties of the FDM fabricated PLA, PGP/PLA, and PGF/PLA composites. Error bars represent standard deviation. Significance was marked with: * ($p < 0.05$, $n = 5$), ** ($p < 0.01$, $n = 5$) in black (strength) and red (modulus). [Color figure can be viewed at wileyonlinelibrary.com]

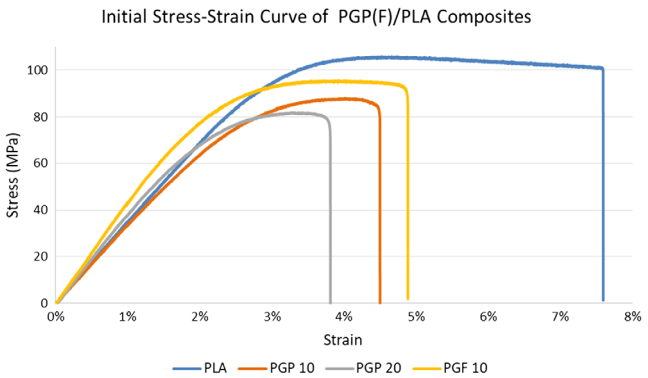

Figure 4. Typical stress–strain curves of the three-point bending test of the FDM fabricated PLA, PGP/PLA, and PGF/PLA composites. [Color figure can be viewed at wileyonlinelibrary.com]

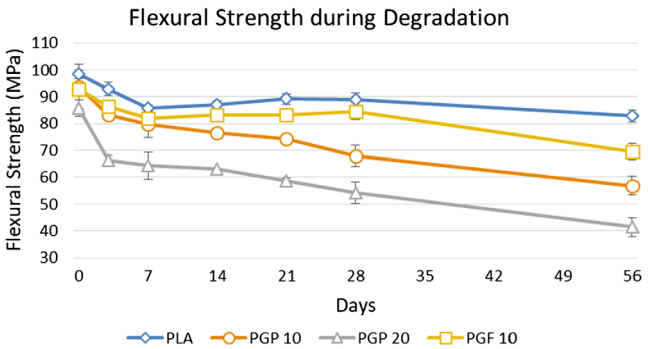

Figure 5. Flexural strength of the FDM fabricated PLA, PGP/PLA, and PGF/PLA composites after specific days of *in vitro* degradation in PBS. Error bars represent standard deviation. [Color figure can be viewed at wileyonlinelibrary.com]

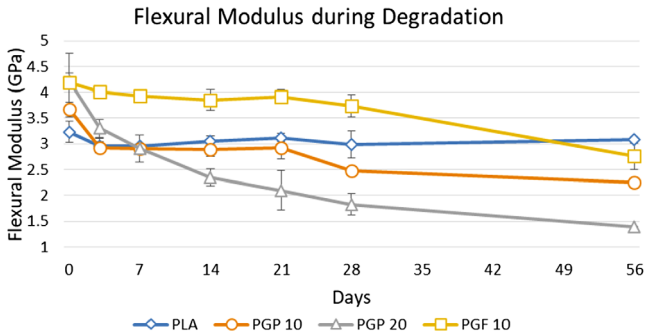

Figure 6. Flexural modulus of the FDM fabricated PLA, PGP/PLA, and PGF/PLA composites after specific days of *in vitro* degradation in PBS. Error bars represent standard deviation. [Color figure can be viewed at wileyonlinelibrary.com]

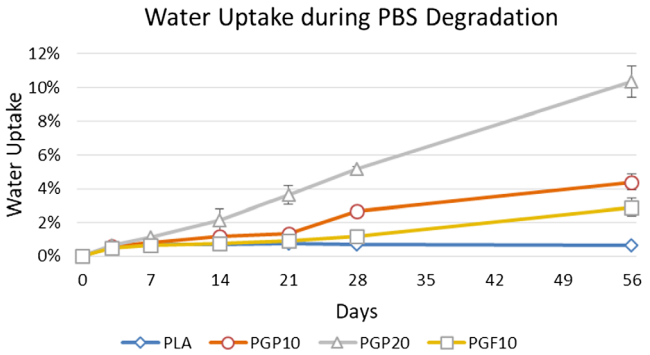

Figure 7. Water uptake profile of the FDM fabricated PLA, PGP/PLA, and PGF/PLA composites after specific days of *in vitro* degradation in PBS. Error bars represent standard deviation. [Color figure can be viewed at wileyonlinelibrary.com]

specimens exhibited the greatest ductility (ultimate strain 7.15 ± 0.33%), followed by the PGF 10 (4.60 ± 0.65%), the PGF 10 (4.54 ± 0.39%), and finally the PGP 20 (3.75 ± 0.32%) composites.

Mechanical Properties after Aqueous Degradation

The flexural properties after immersion in PBS are shown in Figures 5 and 6. Property degradation was evident at 3 days of immersion in PBS. Specifically, the flexural strength and modulus of PGP 20 composites reduced markedly to 77% (66.42 ± 1.76 MPa) and 79% (3.31 ± 0.18 GPa) of the virgin properties, respectively, and both were found statistically significant changes ($p < 0.05$, $n = 3$).

Following the initial, relatively large drop, the mechanical properties followed a more steady reduction. For unreinforced PLA specimens, the strength and modulus more or less maintained their Day 3 properties while the particulate and milled fiber composites exhibited an approximately linear reduction in strength and modulus with respect to time.

As for the particulate reinforced composites, progressive reduction of flexural properties was evident. While the initial flexural modulus of both particulate reinforced specimens was higher than pure PLA before degradation, the values dropped below those of PLA after 7 days of immersion in PBS. By Day 28, the strength and modulus retention were, respectively, 73 and 70% for PGP 10 composites, and 63%/44% for the PGP 20 composites, suggesting that higher particulate loadings accelerated degradation. At the end of 56-day period, the PGP 10 composites retained approximately 60% of initial strength and while the PGP 20 composites maintained only 48% of their initial strength and 34% of initial modulus.

For the PGF 10 composites, 92 and 91% of the initial flexural strength/modulus remained on Day 28, and the modulus was still superior to those of unreinforced PLA, suggesting that the milled fibers provided better property retention than the particulate composites. However, by Day 56, only 75 and 68% of initial strength and modulus were retained in the PGF 10 composites. These values indicated a more severe loss of mechanical properties during Days 28–56, in contrast to the particulate composites that exhibited more severe degradation over the first 28 days. Overall, the flexural strength and modulus of PGF 10 composites remained superior to those of the equivalent particulate composites.

Water Uptake

Water uptake profiles are shown in Figure 7. For PLA specimens, water uptake was evident by Day 3, and more or less stabilized at 0.7%. The water uptake of both particulate composites progressively increased during the 56-day degradation period, with greater uptake at the higher particulate loading. The final water contents reached 4.4 and 10.4% for PGP 10 and PGP 20 composites, respectively. The water uptake of PGF 10 composites was more modest (1.20%) over the first 28 days, increasing to 2.90% by Day 56, indicating that milled fiber composites had a generally lower water uptake propensity compared to those with particulate reinforcement.

pH Values of Immersion Media

The pH histories of the PBS immersion media for the various specimen types are shown in Figure 8. Starting from 7.40, the pH value of PBS immersing PLA did not change significantly during the 56-day degradation period. The phosphate glass reinforced composites, however, caused the pH to fall progressively, for the PGP 10 group dropping to 7.21 by Day 28 and 7.01 by Day 56. The

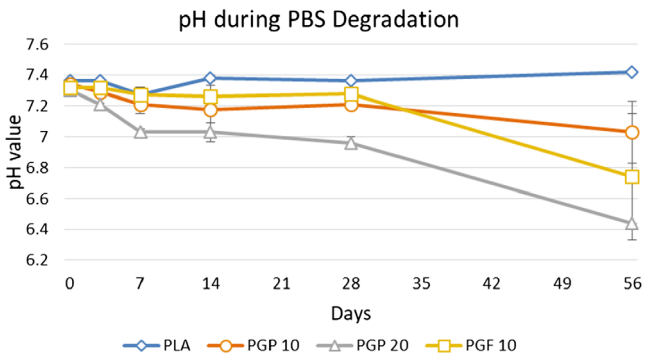

Figure 8. pH profile of PBS immersing the FDM fabricated PLA, PGP/PLA, and PGF/PLA composites after specific days of *in vitro* degradation. Error bars represent one standard deviation. [Color figure can be viewed at wileyonlinelibrary.com]

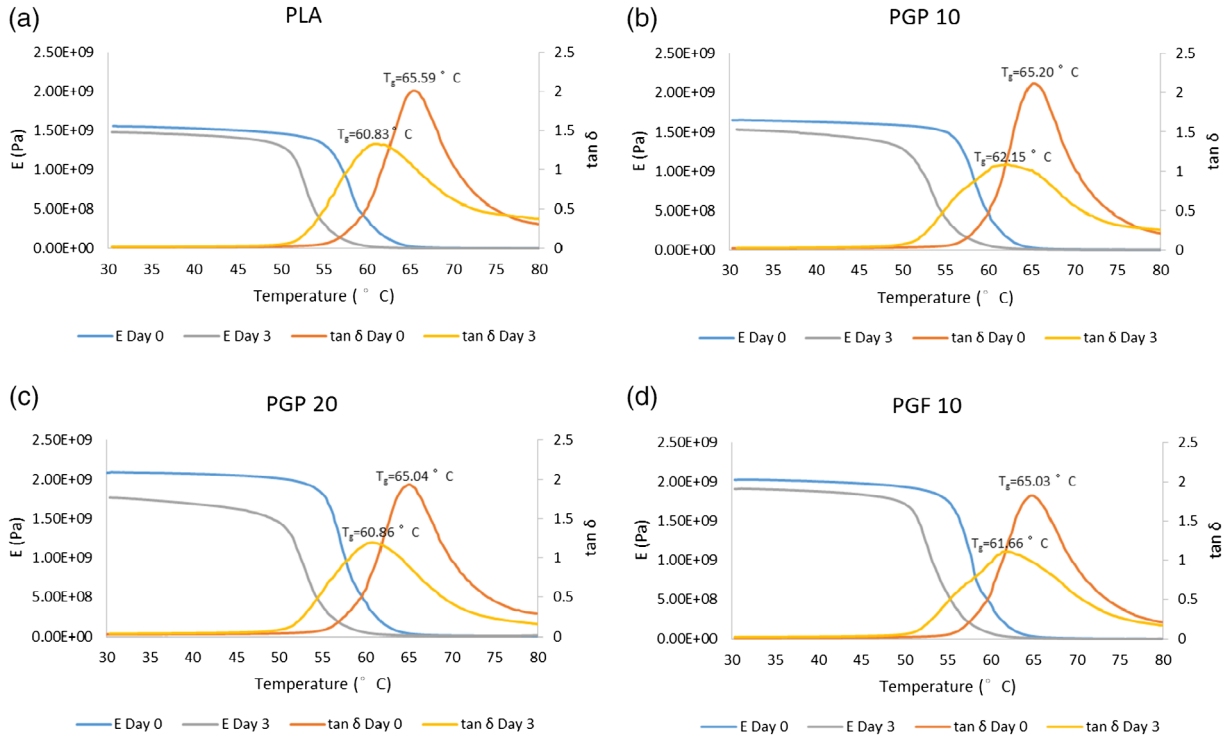

Figure 9. DMA results of (a) PLA, (b) PGP 10, (c) PGP 20, and (d) PGF 10 composites, based on single cantilever—temperature scanning mode. [Color figure can be viewed at wileyonlinelibrary.com]

particulate composites exhibited more dramatic changes; for PGP 20, the pH dropped below 7 by Day 28 and reached 6.44 by Day 56. The PGF 10 composites behaved similarly with accelerated change in pH during the latter part of the degradation period.

Dynamic Mechanical Analysis

DMA was carried out to monitor storage modulus (E) and glass transition temperature (T_g) after 3 days of *in vitro* degradation. Curves of storage modulus (E) and loss factor (δ) are shown in Figure 9. In general, the storage modulus of specimens increased with the incorporation of either particulate or milled fiber reinforcement, and the results followed the same sequence (E: PGP 20 > PGF 10 > PGP 10 > PLA) as obtained from three-point bending test. The glass-transition temperature reduced slightly with the incorporation of phosphate glass fillers. After 3 days of immersion in PBS, the initial storage modulus reduced, and the onset of storage modulus reduction occurred at lower temperatures for all specimens after degradation.

SEM and EDS

SEM images of fracture surfaces of specimens are shown in Figure 10. Images in the left column [Figure 10(a,c,e,g)] are the polished cross sections of virgin specimens. The PLA surface (a) exhibits a series of regular white in the polished cross sections. These represent nonbonded areas between adjacent extrusions and are intrinsic defects associated with FDM. Similar features can be identified in Figure 10(b,f,h) as trapezoidal voids which are highlighted by triangles and parallelogram. For the particulate composites, it was clear that the polyhedral particulate dispersion was fairly even (c, e), with more particles visible as the PGP content increased to 20 wt %. In the polished cross section of PGF 10, the fibers are clearly visible and well distributed. As the polished surfaces were perpendicular to the FDM extrusion path, the more or less circular fiber section indicates close alignment with the direction of extrusion.

As for the pristine fractured surfaces of virgin specimens in the right column [Figure 10(b,d,f,h)], it is evident that many of the glass particles have disbonded from the PLA matrix during the fracture event, as evidenced by the witness hollows as well as the voids surrounding the residual glass fragments (marked by eclipses). The evidence suggests that the interfacial strength between glass particles and the PLA was relatively weak. Meanwhile, smooth and circular voids (marked by arrows) were also evident, and these were likely result of air entrainment during the water cooling process of filament making procedures. Figure 10 (h) shows similar void, also evidence of fiber pull-out for the milled fiber specimens which again supports the likelihood of rather limited interfacial shear strength.

Pristine fractured surfaces of specimens degraded for 28 days are presented in the left column of Figure 11(a,c,e,g). No significant difference was noted from the pure PLA specimens before and after degradation. The fracture surfaces of degraded PGP 10 and PGP 20 composites were similar to those before degradation.

The right column in Figure 11(b,d,f,h) shows the pristine fracture surfaces of specimens after 56 days of degradation. Similarly, no significant difference was seen in the fractured surface of the PLA. For the composites reinforced with glass particles, further pitting was evident on the fracture surfaces, suggesting more pronounced interface failure as the PGP/PLA interfacial strength was further weakened.

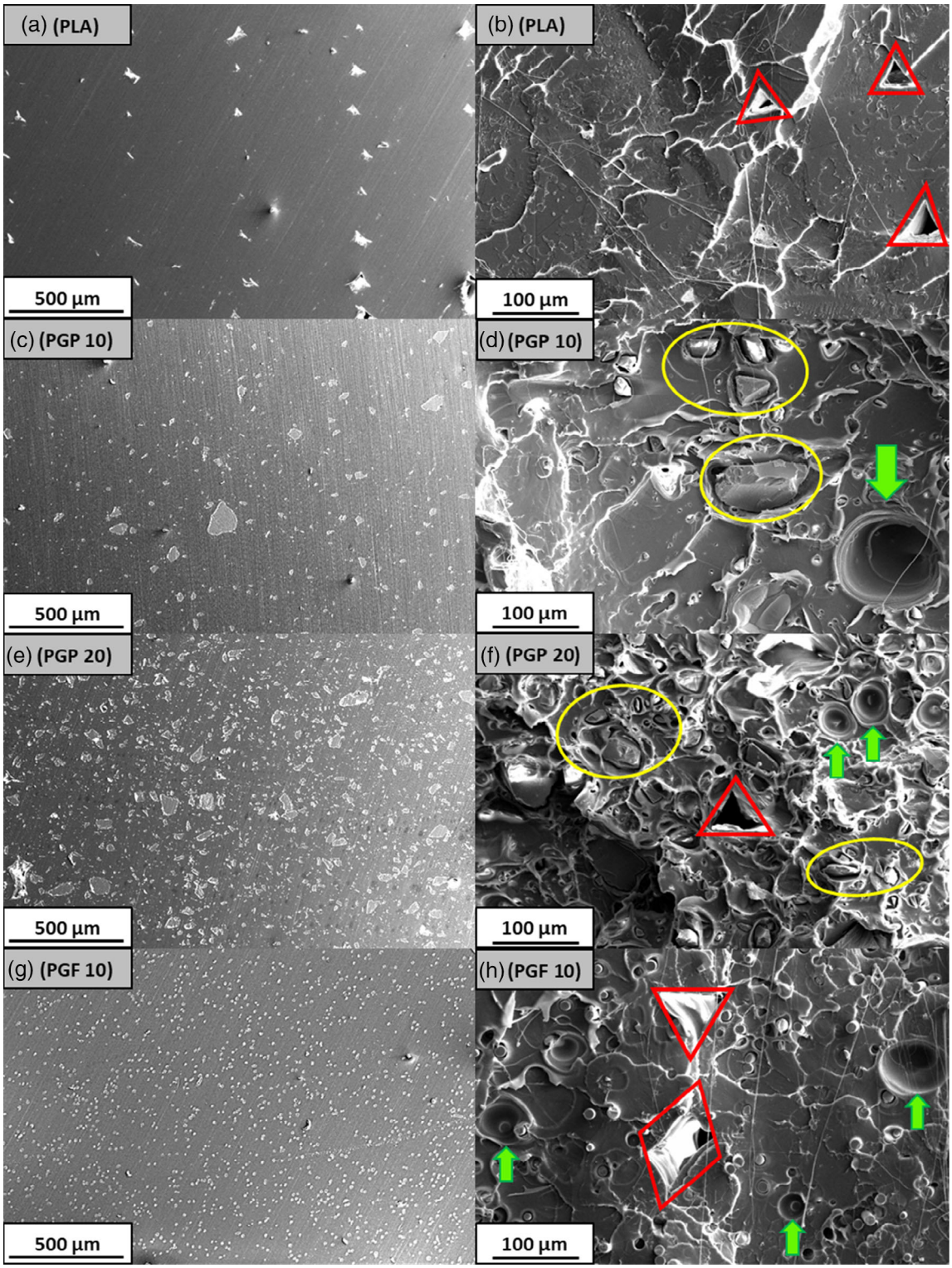

Figure 10. SEM images of polished/pristine fractured surfaces of virgin PLA (a,b); PGP 10 (c,d); PGP 20 (e,f); and PGF 10 (g,h) composites. [Color figure can be viewed at wileyonlinelibrary.com]

Moreover, round excrescences were observed in the fractured surfaces. With higher loading of glass in the PGP 20 composites, the resultant excrescences were larger. In the fractured surface of PGF 10 specimens, pulled out fibers, trapped air bubbles, as well as excrescences humps all presented on the fractured surfaces. Figure 12 indicates that the excrescences were the fusion of degradation products from the phosphate glass, as both residual PGP and PGF can be seen fused into the excrescences. The EDS

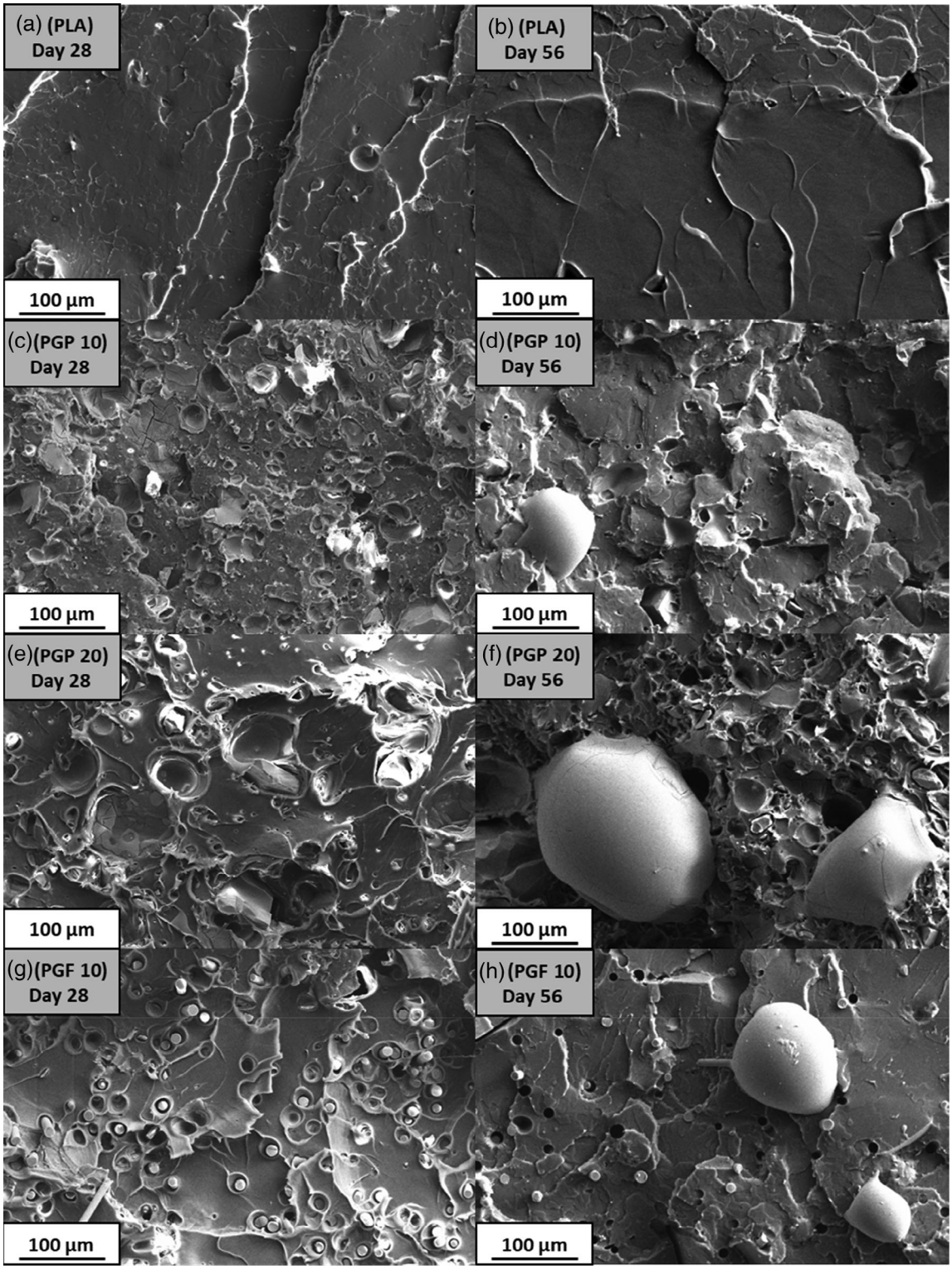

Figure 11. SEM images of pristine fractured surfaces of PLA (a,b); PGP 10 (c,d); PGP 20 (e,f); and PGF 10 (g,h) degraded at 37 °C in PBS for 28/56 days.

results in Figure 13 show that the relative atomic ratio among Mg, Ca, and Fe of excrescences were close to those of virgin PGPs/PGFs. The reduced Mg along with increased Fe content was the result of degradation of magnesium oxide which took place at a higher rate than the iron oxide.

Single extruded paths of PGP 10 and PGF 10 composites in horizontal direction were examined under SEM. Figure 14(a) was taken from a PGP 10 composite specimen. Glass particles are found evenly dispersed in the composites and no preferred location or alignment of PGP can be observed from the image. For the

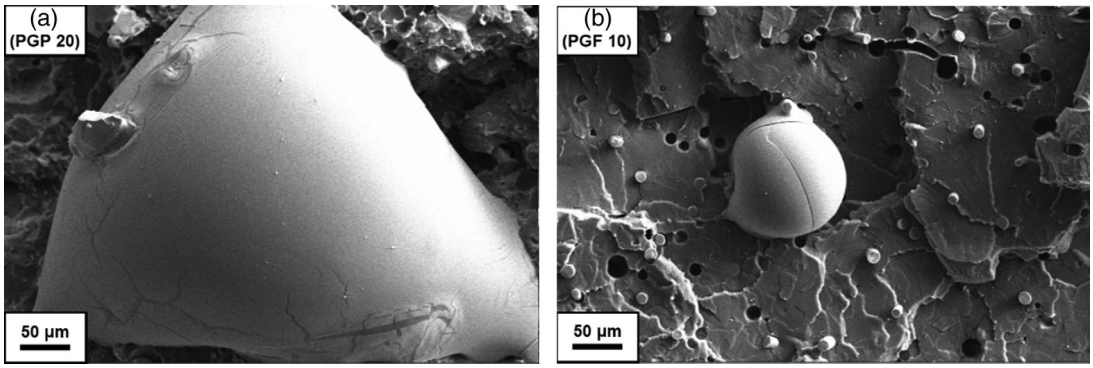

Figure 12. SEM images showing the fusion of PGPs (a) and PGFs (b) into excrescences, captured on Day 56.

same model fabricated with PGF 10 composite [Figure 14(b)], it was found that a certain portion of the fibers were in the same direction of the extruded path, indicating alignment of milled PGFs in the direction of FDM extrusion.

DISCUSSION

Initial Structural and Mechanical Properties

Comparing with PLA specimens, the incorporation of glass particles led to improved flexural modulus, reduced flexural strength, and reduced strain at break, and the effects were intensified with increased PGP loading. These are logical and well reported effects from the addition of rigid fillers.[23] Embrittlement and strength reduction is associated with of stress concentration and low interfacial strength.[23] It is likely here that the stress concentration effect was augmented by the incorporation of particulate with sharp corners. With increased filler loading, stress concentration sites also increased and led to more pronounced strength reduction and the same effect on strain at failure.[23] Strength reduction was probably also contributed to by the likelihood of higher voids fraction in the composites, including the air trapped in during water cooling, and the gaps between adjacent extruded paths associated with decreased propensity to flow as the particulate contents in molten feedstock increased. The strain at break of materials reduced with increasing glass content, indicating that the rigid particulate reinforcements were unable to arrest crack growth. The reduced strength along with reduced strain at break suggests that the bonding between the glass particles and PLA matrix was rather weak, as the strong interfacial bonding generally enhances the strength and often the toughness of composites.[23]

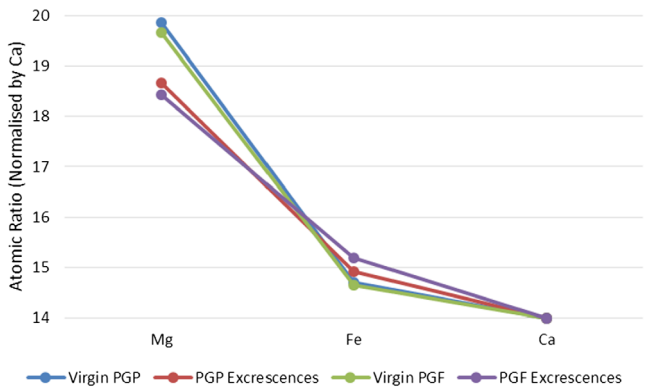

Figure 13. Relative atomic ratio among Mg, Fe, and Ca normalized by Ca, as examined using EDS. [Color figure can be viewed at wileyonlinelibrary.com]

When comparing to the particulate filler with the same weight fraction of milled fibers, it is clear that the latter were more effective in improving the modulus of composites, whereas the strength and failure strain were similar. As reported in previous studies, the incorporation of fiber reinforcements generally contributed to improved strength in additively manufactured polymer composites,[24–26] which is in contrary to the results in this study. The tensile strength of short fiber reinforced polymer composites is highly related to the loading, orientation distribution, and the length distribution of fibers. For the length distribution, it is reported by Fu *et al.* that as the median/mode of fiber length increase, fibers are more likely to approach their critical length in composites, resulting in improved mechanical strength.[27] Thomason *et al.* studied the properties of compression molded glass fiber/polypropylene composites and the tensile/flexural strength of composites reduced when very short fibers (average length = 100 μm) were added into composites.[28] In this study, the average fiber length was only 54 μm, with the median and mode of fiber length being even lower. Moreover, it is previously reported that the incorporation of 10 mm PGFs in PLA would not effectively improve the strength comparing to PLA alone.[29] In summary, the fiber length here was too short to enable the fibers to be loaded to their full tensile strength before an interfacial failure would occur, as demonstrated elsewhere using discontinuous carbon fibers at different lengths.[24,30] Similarly, the interfacial bonding between PGF and PLA was not sufficiently strong, as indicated by the reduced strength and strain at break.

The pronounced modulus enhancement arising from the addition of milled fibers is of course a direct mixture effect from the addition of a high modulus phase to the PLA. The high aspect ratio combined with a high level of alignment along the filament leads to a significant improvement in the axial stiffness.[16,31] The PGPs clearly have substantially lower aspect ratios and no clear evidence of alignment with the filament axis. As polymer melt solidified, the fiber alignment was preserved in the solidified product.[32] This phenomenon was observed in several studies[24,33] and recently demonstrated with simulation of the FDM process.[34]

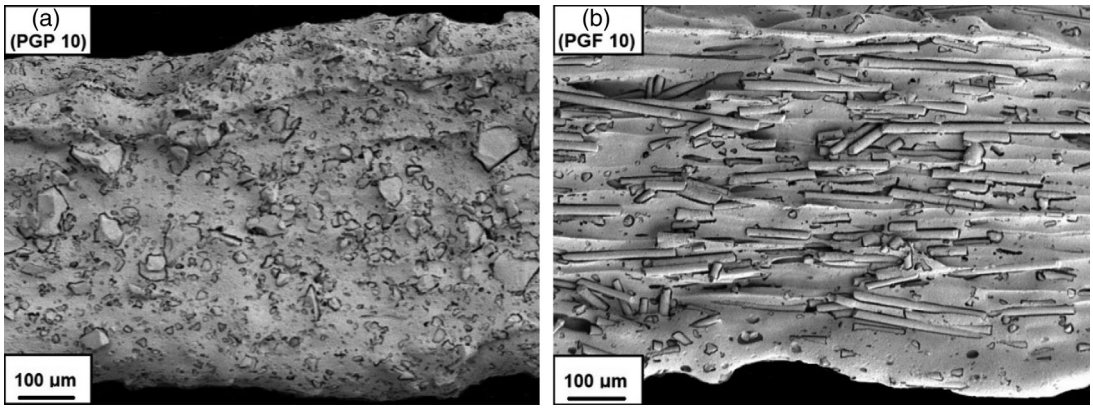

Figure 14. SEM images of single, horizontally extruded paths of PGP 10 composites (a) and the PGF 10 composites (b).

Observation of the microscopy specimens introduced earlier confirmed the fiber alignment effect.

Hydrolytic Degradation

The mechanical properties of all specimens were reduced during the first 3 days of degradation. Specifically, over 20% loss of strength and modulus were recorded from the PGP 20 composites. Meanwhile, only minor pH reduction was recorded in the immersion media, suggesting that the significant dissolution of phosphate glass was unlikely to have taken place.

The initial reduction of mechanical properties is attributed to the PLA matrix becoming plasticized by water ingress. Water-induced plasticization is a well-reported phenomenon for polyesters including PLA.[6] As polyesters are immersed in aqueous media, the low-molecular-weight water infuses into the network of high-molecular-weight polymers, increasing the free volume in the polymer at the molecular level.[35] Consequently, the mobility of the polymer backbone increases while the rigidity of polymer structure reduces, leading to lowered elastic modulus and glass transition temperature.[36] Rodriguez *et al.* immersed compression molded PLA disks in 70 °C distilled water (pH = 5.4) for 10 days and reported that glass-transition temperature (T_g) a reduction from 61 °C to around 50 °C after 3 days of immersion, and a weight-average molecular weight reduced by 80%.[37] Similarly, Kikkawa *et al.* noted that comparing to counterparts conditioned and tested in a vacuum, the PLA thin films immersed in water had lower T_g reductions and higher molecular mobility at their surfaces, demonstrating the role of water as a plasticizer.[38] In this study, the T_g of all degraded specimens dropped compared to those before immersion. Along with the reduced modulus recorded from both three-point bending test and DMA, it is very likely that plasticization of specimens took place within 3 days of degradation. Meanwhile, more pronounced strength reduction was found from PGPs reinforced composites. This is possibly the result of compromised interfacial strength due to hydrolysis.[39]

From Day 3 on, there was only a minor reduction in the flexural properties as well as pH of immersion media for PLA. It is known that the degradation rate of PLA in benign environments (e.g., 37 °C deionized water/PBS immersion) is rather slow.[40] Thus, the PLA exhibited good property retention. In contrast, progressive reductions of mechanical properties were observed in both the particulate and milled fiber composites beyond Day 3. For the particulate reinforced composites, the reduction of flexural properties, the incremental water uptake, and reduction of pH in the immersion media all point clearly to hydrolytic degradation of the phosphate glass and this effect is magnified as the filler loading increases since there is a greater surface area of glass available to the media.[41] The milled fiber composites degraded

Table II. Comparison of Mechanical Properties among Human Bones, PGF 10, Continuous PGF (cPGF)/PLA Composites PLLA

Materials/skeletal structures	Reinforcement ratio	Process	Strength	Modulus	Reference
Human cortical bones	—	—	50–150 MPa	6–20 GPa	16,42
Human cancellous bones	—	—	10–20 MPa	0.05–0.50 GPa	16
PGF 10 (Day 0)	10% (weight)	FDM[a]	92.28 MPa	4.10 GPa	This work
PGF 10 (Day 28)	10% (weight)	FDM	84.63 MPa	3.74 GPa	This work
PGF 10 (Day 56)	10% (weight)	FDM	69.47 MPa	3.03 GPa	This work
cPGF/PLA (Day 0)	20% (volume)	CM[b]	~180 MPa	~12 GPa	42
cPGF/PLA (Day 28)	20% (volume)	CM	~70 MPa	~3 GPa	42
PLLA (Day 0)	—	IM[c]	64.8 MPa	4 GPa	43

[a] FDM, fused deposition modeling.
[b] CM, compression molding.
[c] IM, injection molding.

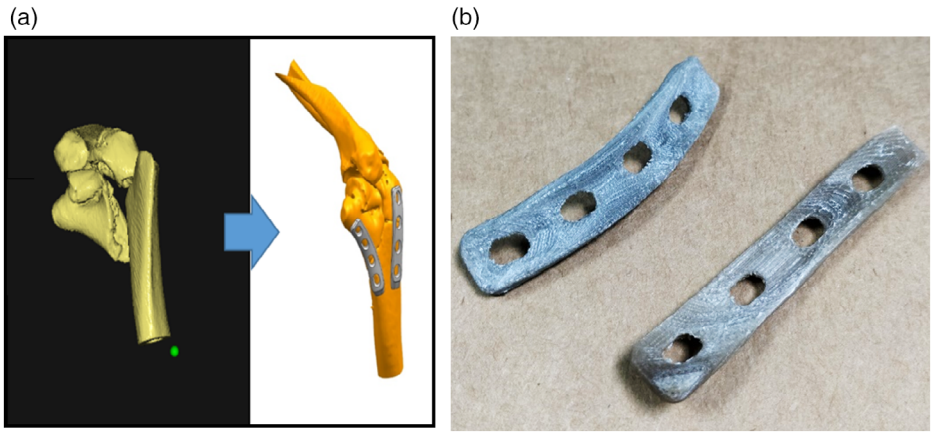

Figure 15. The CT data of elbow that the digital model of customized fixation plates was designed upon (a), and the additively manufactured demo parts of customized PGF 10 fixation plates for elbow fracture (b). [Color figure can be viewed at wileyonlinelibrary.com]

more slowly compared to the particulate composites and a higher retention of mechanical properties was evident, along with lower water uptake. A possible reason is that the PGF bundles were coated with sizing after the production, which served as a barrier against hydrolytic degradation, thus contributing to reduced degradation rate of resultant composites.

General Discussion

The purpose of this study was to examine the potential of additively manufactured composites for use as bone fixation implants. The mechanical properties of human bone, additively manufactured PGF 10 composites, and a continuous PGF/PLA composite are listed in Table II. Comparing with the mechanical properties of cortical bones, the (dry) flexural strength of the PGF 10 composite is a close approximation, while the flexural modulus is much lower. Stiffness matching is recognized as the "gold standard" for bone fixation implants, as fixation implants with such mechanical properties are strong and stiff enough for the load-bearing activities without leading to "stress shielding." As such, it is probably necessary to consider the use of higher/longer fiber loading for this type of application.

In contrast, continuous PGF/PLA composites are more suitable for the fixation of load-bearing bones due to the superior initial modulus, which is attributed to the incorporation of continuous fibers that lead to effective improvement of stiffness via better alignment and a higher volume fraction. However, it is also seen that the flexural modulus of such materials reduced by ~80% after 28 days of degradation, whereas the PGF 10 composites lost ~30% of initial flexural modulus even after a prolonged degradation period of 56 days. The rapid reduction of flexural modulus was attributed to the exposure of fiber ends in degradation media, which allowed water to diffuse into the composites.[17] More importantly, the continuous fiber reinforcements were later "wicked" by the water, leading to accelerated hydrolytic degradation.[17] On the contrary, the milled PGFs within the PGF 10 composites were better encapsulated by the polymer, thus protected from direct exposure to degradation media. On top of that, it shall be mentioned that the fabrication of continuous PGF reinforced composites were currently limited to molding techniques such as compression molding and *in situ* polymerization,[17,44] and the use of mold constrained the geometries of composites produced. In contrast, the PGF 10 composites in this study were additively manufactured via a free-form fabrication process, so the implants with complex shape and size can be obtained straightforwardly, with low demand on further shaping/machining.

Based on the consideration of both the initial mechanical properties and the facility to produce composites with desired geometries straightforwardly, the additive manufacturing of PG/PLA composites exhibits good potential in the making of patient-specific fixation implants for bone that has low demand for load-bearing, for example, zygoma,[45] ankle,[46,47] and maxilla.[48] These bones have been previously reported to be successful restored using PLA-based biodegradable fixation devices. Compared to PLA alone, it was demonstrated that the incorporation of PGF enhanced the flexural modulus of implants. It is also anticipated that the degradation of PGF releases magnesium, calcium, and phosphate to upregulate bone regrowth. Moreover, the FDM process allows fixation implants with customized geometries to be built directly, and may remove the need for contouring of implants for anatomic fit during the operation.[47]

As a proof of concept, a pair of fixation plates designed for the fixation of elbow fractures were built and shown in Figure 15. The models of fixation plates indicated to repair the ankle fracture were designed based on the computed tomography (CT) data acquired. Clearly, before clinical trials, further research is required to investigate whether these materials are compatible with biological system, and function properly in the bone-fracture healing process.

The results of this preliminary research also indicate that the additively manufactured PG/PLA composites can be further enhanced for their properties and utilized in other fields. For the milled fiber composites, the mechanical properties were found to be limited by the fiber length as well as the internal voids. The feasibility of incorporating longer fibers and reducing internal voids are obvious next steps. It is also noticed that particulate reinforced composites suffered from rapid loss of mechanical properties. Meanwhile, the reducing pH value of the immersion media was a strong proxy for glass degradation. While the

degradation of phosphate glass needs to be controlled in order to maintain mechanical properties, the effect may be utilized for the efficient release of degradation that benefits the bone growth activities which may lead to customized bone tissue engineering scaffolds for repair of bone defects.

CONCLUSIONS

PG/PLA composites were additively manufactured via FDM. The mechanical properties and degradation behavior of composites were investigated. It was found that with the incorporation of PGPs resulted in reduced flexural strength and improved flexural modulus of the composites, and the trend was intensified with increased particulate loadings. Comparing to particulate composites of same weight fraction, milled PGFs were more effective in improving the flexural modulus of composites. During aqueous conditioning, the degradation rate of particulate reinforced composites increased with higher filler loadings, whereas the milled fiber composites showed better retention of mechanical properties comparing to those with same weight fraction of particulates. The proof-of-concept customized bone fixation plates were additively manufactured using the milled fiber composites, yet more work is required to improve the load-bearing ability of composites and confirm the compatibility of additively manufactured PG/PLA composites for customized bone fracture fixation.

ACKNOWLEDGMENTS

This research is funded by the Ningbo 3315 Innovation Team Scheme of "Marine Composites Development and Manufacturing for Sustainable Environment", as well as the Ningbo S&T Bureau Ningbo International Collaboration Project (project code: 2017D10012).

REFERENCES

1. Egol, K. A.; Kubiak, E. N.; Fulkerson, E.; Kummer, F. J.; Koval, K. J. *J. Orthop. Trauma*. **2004**, *18*, 488.
2. Daniels, A. U.; Chang, M. K. O.; Adirano, K. P.; Heller, J. *J. Appl. Biomater.* **1990**, *1*(57), 331.
3. Koh, J.; Berger, A.; Benhaim, P. *J. Hand Surg. Am.* **2015**, *40*, 1703.
4. Fouad, H. *Med. Eng. Phys.* **2010**, *32*, 783.
5. Charles, L. C.-H.; Man-Hong, C.; Samuel, L. K.-K.; Chun-Man, M. *J. Orthop. Trauma Rehabil.* **2017**, *23*, 25.
6. Middleton, J. C.; Tipton, A. J. *Biomaterials*. **2000**, *21*, 2335.
7. Harith, H.; Malekani, J.; Schmutz, B.; Schuetz, M.; Yarlagadda, P. K. D. V. *Proc. Inst. Mech. Eng. Part L: J. Mater. Des. Appl.* **2015**, *230*, 282.
8. Henkel, J.; Woodruff, M. A.; Epari, D. R.; Steck, R.; Glatt, V.; Dickinson, I. C.; Choong, P. F.; Schuetz, M. A.; Hutmacher, D. W. *Bone Res.* **2013**, *1*, 216.
9. Holzapfel, B. M.; Chhaya, M. P.; Melchels, F. P.; Holzapfel, N. P.; Prodinger, P. M.; von Eisenhart-Rothe, R.; van Griensven, M.; Schantz, J. T.; Rudert, M.; Hutmacher, D. W. *Sarcoma*. **2013**, *2013*, 153640.
10. Probst, F. A.; Hutmacher, D. W.; Muller, D. F.; Machens, H. G.; Schantz, J. T. *Handchir. Mikrochir. Plast. Chir.* **2010**, *42*, 369.
11. Esposito Corcione, C.; Gervaso, F.; Scalera, F.; Montagna, F.; Sannino, A.; Maffezzoli, A. *J. Appl. Polym. Sci.* **2017**, *134*, 44656.
12. Serra, T.; Planell, J. A.; Navarro, M. *Acta Biomater.* **2013**, *9*, 5521.
13. Poh, P. S. P.; Hutmacher, D. W.; Stevens, M. M.; Woodruff, M. A. *Biofabrication*. **2014**, *5*, 045005.
14. Park, J.; Lee, S. J.; Jo, H. H.; Lee, J. H.; Kim, W. D.; Lee, J. Y.; Park, S. A. *J. Ind. Eng. Chem.* **2017**, *46*, 175.
15. Korpela, J.; Kokkari, A.; Korhonen, H.; Malin, M.; Narhi, T.; Seppala, J. *J. Biomed. Mater. Res. B Appl. Biomater.* **2013**, *101*, 610.
16. Colquhoun, R.; Tanner, K. E. *Biomed. Mater.* **2015**, *11*, 014105.
17. Ahmed, I.; Jones, I. A.; Parsons, A. J.; Bernard, J.; Farmer, J.; Scotchford, C. A.; Walker, G. S.; Rudd, C. D. *J. Mater. Sci. Mater. Med.* **2011**, *22*, 1825.
18. Sin, L. T.; Rahmat, A. R.; Rahman, W. A. W. A. In Polylactic Acid; Sin, L. T.; Rahmat, A. R.; Rahman, W. A. W. A., Eds., William Andrew Publishing: Oxford, UK, **2013**.
19. Han, N.; Ahmed, I.; Parsons, A. J.; Harper, L.; Scotchford, C. A.; Scammell, B. E.; Rudd, C. D. *J. Biomater. Appl.* **2013**, *27*, 990.
20. Haglin, J. M.; Eltorai, A. E.; Gil, J. A.; Marcaccio, S. E.; Botero-Hincapie, J.; Daniels, A. H. *Orthop. Surg.* **2016**, *8*, 417.
21. Zhu, C. *Ceram. - Silikaty*. **2018**, *62*, 111.
22. Zhu, C.; Liu, J.; Huang, S.; He, L.; Cong, X.; Tan, C.; Rudd, C.; Liu, X. *New J. Glass Ceram.* **2017**, *07*, 100.
23. Fu, S.-Y.; Feng, X.-Q.; Lauke, B.; Mai, Y.-W. *Compos. Part B Eng.* **2008**, *39*, 933.
24. Tekinalp, H. L.; Kunc, V.; Velez-Garcia, G. M.; Duty, C. E.; Love, L. J.; Naskar, A. K.; Blue, C. A.; Ozcan, S. *Compos. Sci. Technol.* **2014**, *105*, 144.
25. Negi, S.; Dhiman, S.; Sharma, R. K. *Measurement*. **2015**, *68*, 205.
26. Carneiro, O. S.; Silva, A. F.; Gomes, R. *Mater. Des.* **2015**, *83*, 768.
27. Fu, S.-Y.; Lauke, B. *Compos. Sci. Technol.* **1996**, *56*, 1179.
28. Thomason, J. L.; Vlug, M. A.; Schipper, G.; Krikor, H. G. L. T. *Compos. A: Appl. Sci. Manuf.* **1996**, *27*, 1075.
29. Felfel, R. M.; Ahmed, I.; Parsons, A. J.; Walker, G. S.; Rudd, C. D. *J. Mech. Behav. Biomed. Mater.* **2011**, *4*, 1462.
30. Ning, F.; Cong, W.; Qiu, J.; Wei, J.; Wang, S. *Compos. Part B: Eng.* **2015**, *80*, 369.
31. Jones, J. R. *Acta Biomater.* **2013**, *9*, 4457.
32. Guell, D.; Bénard, A. In Flow-Induced Alignment in Composite Materials; Papathanasiou, T. D.; Guell, D. C., Eds., Woodhead Publishing: Cambridge, England, **1997**.

33. Gray, R. W., IV; Baird, D. G.; Helge Bøhn, J. *Polymer Composites*. **1998**, *19*, 383.
34. Heller, B.; Smith, D. E.; Jack, D. A. 30th Technical Conference on Composite Materials, East Lansing, MI, **2015**.
35. Hodge, R. M.; Bastow, T. J.; Edward, G. H.; Simon, G. P.; Hill, A. J. *Macromolecules*. **1996**, *29*, 8137.
36. Levine, H.; Slade, L. In Water Science Reviews 3: Water Dynamics; Franks, F., Ed., Cambridge University Press: Cambridge, UK, **1988**.
37. Rodriguez, E. J.; Marcos, B.; Huneault, M. A. *J. Appl. Polym. Sci.* **2016**, *133*, 44152.
38. Kikkawa, Y.; Fujita, M.; Abe, H.; Doi, Y. *Biomacromolecules*. **2004**, *5*, 1187.
39. Lin, P.-L.; Fang, H.-W.; Tseng, T.; Lee, W.-H. *Mater. Lett.* **2007**, *61*, 3009.
40. Höglund, A.; Odelius, K.; Albertsson, A.-C. *ACS Appl. Mater. Interfaces*. **2012**, *4*, 2788.
41. Navarro, M.; Engel, E.; Planell, J. A.; Amaral, I.; Barbosa, M.; Ginebra, M. P. *J. Biomed. Mater. Res. A*. **2008**, *85*, 477.
42. Sharmin, N.; Hasan, M. S.; Parsons, A. J.; Rudd, C. D.; Ahmed, I. *J. Mech. Behav. Biomed. Mater.* **2016**, *59*, 41.
43. Farah, S.; Anderson, D. G.; Langer, R. *Adv. Drug Deliv. Rev.* **2016**, *107*, 367.
44. Qu, X.; Xia, P.; He, J.; Li, D. *Mater. Lett.* **2016**, *185*, 554.
45. Bergsma, J. E.; de Bruijn, W. C.; Rozema, F. R.; Bos, R. R. M.; Boering, G. *Biomaterials*. **1995**, *16*, 25.
46. Eitenmüller, J.; David, A. A.; P.; Muhr, G. *Chirurg.* **1996**, *67*, 413.
47. Kukk, A.; Nurmi, J. T. *Foot Ankle Surg.* **2009**, *15*, 192.
48. Haers, P. E.; Suuronen, R.; Lindqvist, C.; Sailer, H. *J. Craniomaxillofac. Surg.* **1998**, *26*, 87.